Identification of Potential EGFR Inhibitors for Type 2 Diabetes and Pancreatic Cancer Treatment: A Computational Approach

Ricardo Romero[a]

Abstract: A differential gene expression analysis was performed in two studies of type 2 diabetes on pancreatic samples (Langerhans cells). In both cases the Epidermal Growth Factor Receptor (EGFR) was identified as the top hub gene in the protein-protein interaction networks of the upregulated genes. Functional enrichment analysis revealed that EGFR is also involved in pancreatic cancer signaling pathways. A virtual screening was conducted using EGFR inhibitors from the ZINC20 database. The results were filtered based on binding energies as well as ligands' absorption, distribution, metabolism, excretion, and toxicity (ADMET) properties. To filter the results further, two machine learning models were implemented and trained on a different set of ligands obtained from the ChEMBL database, one for regression and another for classification, to respectively predict pIC50 values and bioactivity class, resulting in six finalist compounds with viable characteristics, in terms of bioactivity and drug likeness, to be developed as EGFR inhibitors. Approved drugs afatinib, erlotinib, and almonertinib were used as controls, and in all cases the finalist compounds obtained better scores than the control drugs.

Keywords: EGFR, type 2 diabetes, pancreatic cancer, virtual screening, machine learning

1 Introduction

Type 2 diabetes (T2D) is a complex and chronic metabolic disorder, caused by both genetic and environmental factors [1, 2, 3]. Its main characteristic is hyperglycemia, which results from impaired insulin secretion, insulin resistance, or both. It is estimated that over 400 million people worldwide are affected by T2D, and its prevalence continues to rise. Other characteristics include obesity, dyslipidemia, hypertension, and inflammation, which have been linked to the development of other complications such as cardiovascular disease, neuropathy, nephropathy and retinopathy.

Several studies have shown that T2D is associated with reduced mass and/or reduced number of β-cells in the pancreatic islets [4, 5], which are clusters of endocrine cells located within the pancreas [6]. These cells are responsible for secreting hormones such as insulin, glucagon, and somatostatin, among others, as well as altered functionality of these cells [7], leading to insufficient insulin release and eventually hyperglycemia. Several genetic variants [8, 9, 10], identified through genome-wide association studies (GWAS), have been associated with the risk of developing T2D by influencing beta-cell function, mass, or response to various stimuli. Overall, the association between T2D and pancreatic islets highlights the importance of studying the underlying molecular mechanisms involved in the pathophysiology of disease onset and progression.

The management of T2D involves lifestyle changes such as diet and exercise, along with pharmacological prescriptions such as metformin, sulfonylureas, DPP4 inhibitors, etc., aiming to reduce blood sugar levels and improve insulin sensitivity [11, 12, 13]. However, these drugs do not stop or reverse the progression of the disease, focusing primarily on sugar control and symptom management. This highlights the need for better theoretical and experimental results that could eventually lead to the development of improved drugs for its treatment.

On the other hand, the Epidermal Growth Factor Receptor (EGFR) is a transmembrane protein also known as ErbB1 or HER1, which plays a critical role in cellular signaling pathways. It belongs to the ErbB family of tyrosine kinase receptors and is expressed on the surface of various cells, including epithelial cells. Activation of EGFR initiates a cascade of intracellular events that lead to cell proliferation, survival, differentiation, and migration. The main features of the human EGFR include its extracellular domain, responsible for recognizing growth factors such as epidermal growth factor (EGF) and transforming growth factor-alpha (TGF-α). Upon binding to its ligand, EGFR undergoes conformational changes that result in dimerization and auto-phosphorylation of specific tyrosine residues within its cytoplasmic kinase domain. This phosphorylation activates downstream signaling pathways involved in the regulation of cell growth, tissue

[a] Departamento de Ciencias Naturales, UAM Unidad Cuajimalpa, Avenida Vasco de Quiroga 4871, Col. Santa Fe Cuajimalpa. Alcaldía Cuajimalpa de Morelos, C.P. 05348, Ciudad de México
Email: rromero@cua.uam.mx

development, wound healing, and maintenance of epithelial tissues. Dysregulation or mutations in EGFR have been associated with various cancers [14], making it an important target for therapeutic interventions, such as targeted therapies and small molecule inhibitors. Although the relation between EGFR and diabetes is not conclusive, there are already studies pointing to their association, such as the proposal of EGFR as a therapeutic target for diabetic kidney disease and insulin resistance [15, 16].

Several FDA-approved drugs [17], specifically designed to inhibit EGFR signaling, have proven to be effective treatments for certain types of cancers, including non-small cell lung cancer (NSCLC), colorectal cancer, and head and neck squamous cell carcinomas. These include Gefitinib (Iressa), which is an EGFR tyrosine kinase inhibitor approved for the treatment of NSCLC. Erlotinib (Tarceva) is another EGFR tyrosine kinase inhibitor indicated for NSCLC and pancreatic cancer. Afatinib (Gilotrif) is an irreversible tyrosine kinase inhibitor targeting both EGFR and HER2, used in NSCLC treatment with specific mutations. Osimertinib (Tagrisso) is a drug approved for advanced or metastatic NSCLC patients who have developed resistance to other EGFR inhibitors due to a T790M mutation. Cetuximab (Erbitux) is a monoclonal antibody targeting EGFR, used in colorectal cancer, head and neck cancer, and some types of lung cancer. These targeted therapies can provide personalized treatment options by selectively blocking EGFR activity or its downstream signaling pathways, leading to improved clinical outcomes for patients with EGFR-driven malignancies.

The objective of this study is to identify suitable compounds to be developed as drugs for a more effective treatment of type 2 diabetes, beyond the currently available drugs for the disease control. To achieve this, it is necessary to first identify, through differential expression analysis and interaction networks, the main hub genes associated with T2D based on pancreatic islet samples. Subsequently, a virtual screening using molecular docking and machine learning, as well as filtering of ADMET properties, will be performed to identify compounds with the best characteristics to proceed to the in vitro phase.

2 Methods and materials

2.1 Data Acquisition and Analysis

Two studies, GSE25724 and GSE196797, were obtained from the Gene Expression Omnibus (https://www.ncbi.nlm.nih.gov/geo) database for the present analysis. These studies were selected based on the following criteria:

- The studies focused on type 2 diabetes using pancreatic islet samples.
- The datasets provided a clear distinction between type 2 diabetes (T2D) and non-T2D (control) samples.
- The gene expression analysis yielded differentially expressed genes suitable for constructing a protein-protein interaction (PPI) rich network.

The purpose of the last requirement will be clarified in the results section. The GSE25724 study data were analyzed online using the GEO2R tool, a differential gene expression analysis tool provided by NCBI for microarray data. The

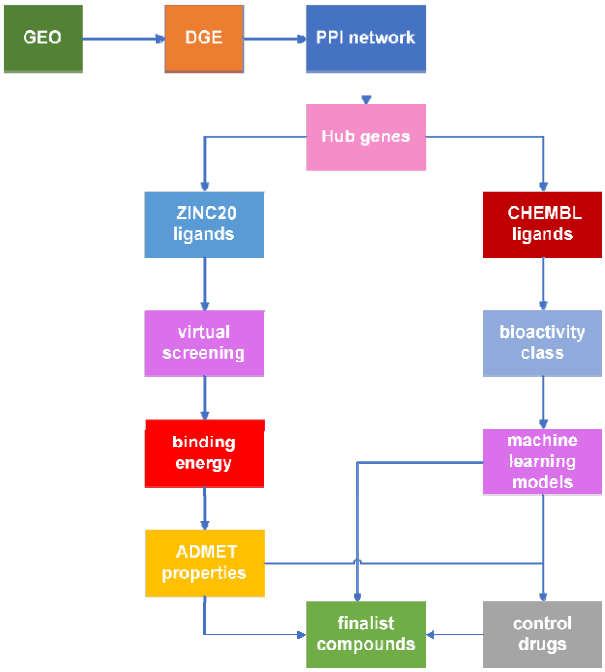

Figure 1. Flowchart of the procedure followed in the present study. The data is obtained from the Gene Expression Omnibus (GEO), and an analysis of differential gene expression (DGE) is performed. The protein-protein interaction (PPI) network is derived, and hub genes are identified. Ligands are obtained from ZINC20, and virtual screening is conducted. The results are filtered based on binding energy and ADMET properties. Simultaneously, machine learning models are trained to further filter compounds based on their bioactivity. The final compounds are compared with control drugs.

analysis compared DT2 (6 samples) versus non-DT2 (7 samples). The data were normalized, and adjusted p-values were calculated using the Benjamini and Hochberg method. Logarithmic transformation and precise weights from the R limma package were applied. Box plots and volcano plots were generated with a significance level of 0.05 and a log2 fold change (log2FC) threshold of zero. The resulting data were downloaded, and genes were selected based on the criteria log2FC > 0 (since only overexpressed genes were of interest) and adjusted p-value < 0.05. The selected genes were then loaded into the STRING server (https://string-db.org) to obtain the PPI network, which was imported into Cytoscape software [18]. Using the CytoHubba plugin [19], the top ten hub genes, based on their degree of interaction, were identified.

For the GSE196797 study, which involved miRNA high-throughput sequencing, the data were not available for analysis using the GEO2R tool. Therefore, the data were analyzed in R Studio using the DESeq2 package [20]

available from the Bioconductor resource center [21]. Normalized gene count data with 2 DT2 samples versus 6 non-DT2 samples were used. Genes with a p-value < 0.05 and log2FC > 0 were selected from the differential expression analysis. Here, the p value was used rather than the adjusted since it was not possible to obtain the later for all genes. The PPI network and top ten hub genes were obtained following the same procedure as the previous study. The datasets and the R script used for analysis are available in the supplementary materials.

2.2 Enrichment Analysis

In order to identify the most significant interactions, the top ten hub genes from the GSE25724 study were selected for enrichment analysis. These genes were chosen based on their strong interaction network, as demonstrated in the results section. To conduct the analysis, the genes were input into the Enrichr database [22, 23] and compared against the KEGG 2021 Human signaling pathways database [24].

To further validate the findings related to the hub genes, transcriptomic analysis was performed using the GeneTrail 3.2 database [25]. The hub genes were uploaded into the database, and alternatively, the study's accession number was provided to obtain the top ten enriched categories. This analysis incorporated data from the Wiki Pathways 2021 Human database [26] and Gene Ontology [27, 28] (GO).

To explore the involvement of miRNAs in diabetes and pancreatic neoplasms, groups of miRNAs associated with the hub genes were obtained from the miRNet database [29, 30]. This was accomplished by analyzing all the miRNAs linked to the hub genes using the miRNA disease database and performing a hypergeometric test.

2.3 Virtual Screening Procedure

The Epidermal Growth Factor Receptor (EGFR) emerged as the top hub gene in both studies. Consequently, the corresponding protein was searched for in the Uniprot database [31]. The entry with accession number P00533 was selected from the filtered results for humans to retrieve the fasta sequence of the protein. Subsequently, the obtained sequence was loaded into the online software protein BLAST from NCBI (https://blast.ncbi.nlm.nih.gov/Blast.cgi) and compared with the Protein Data Bank (PDB) database.

Among the available PDB structures, entry 7SYD [33] was chosen as it exhibited 100% coverage and 99.92% identity. This structure represents the complete extracellular module of EGFR bound to EGF in a juxtaposed conformation, which was determined through electron microscopy (Figure 1). Prior to docking, the structure was stripped of its EGF ligands using USCF Chimera [34] and underwent energy minimization using Swiss PDB-viewer 4.10 [35]. Gasteiger charges were assigned to the structure using Chimera.

For the virtual screening, ligands were downloaded from the ZINC20 database [36]. Ligands targeting the EGFR gene and available for purchase were selected, resulting in an initial set of 550 compounds. However, after extracting, converting sdf files, and performing energy minimization using Open Babel software [37], only 475 functional ligands remained. The energy minimization was carried out using the Amber force field with 5000 steps. Autodock Vina software [38, 39] was employed for the virtual screening, with the coordinates centered at (158, 171.66, 204.89) and a grid size of (20, 20, 150) to cover the entire domain II of the EGFR structure, known to be the active site of the molecule. The energy range was set to 4 with an exhaustiveness value of 10. A cutoff value for energy was established at -8.5 kcal/mol, and only complexes with equal or lower values were considered. This resulted in 130 potential hits from the original set of 475 ligands.

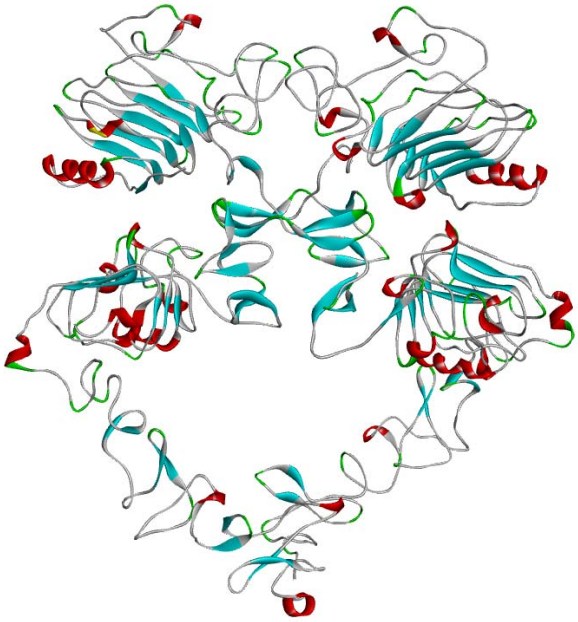

Figure 2. Structure of the Epidermal Growth Factor Receptor (EGFR) molecule, PDB 7SYD, used for molecular docking. The picture shows the structure of the complete extracellular module of EGFR with its ligand EGF removed, in a juxtaposed conformation. The 7SYD structure was obtained through electron microscopy.

2.4 ADMET filtering

The molecular docking results obtained in this study were subjected to further analysis and filtering using various criteria. Firstly, the compounds were loaded into the Swiss ADME database [40] to calculate and retrieve their properties. Subsequently, the compounds were filtered based on their compliance with the drug-likeness rules of Lipinski [41], Ghose [42], Veber [43], Egan [44], and Muegge [45]. An additional solubility filter was applied, requiring that at most one condition among three solubility classes

(ESOL [46], Ali [47], and Silicos-IT) be poorly soluble while the other two should be soluble or moderately soluble. To assess potential toxicological risks, the OSIRIS Property Explorer software (https://www.organicchemistry.org/prog/peo/) was utilized, incorporating filters for mutagenicity, tumorigenicity, irritancy, and reproductive effects. Compounds that passed these filters were recorded, along with their respective solubility, drug-likeness score, and drug score values. Detailed calculation parameters can be found on the program's website.

Upon applying these filters, the number of hits was reduced to 17. To supplement the analysis, control drugs (Afatinib, Almonertinib, Erlotinib, Curcumin, Dimethylcurcumin, and Tirfostin-AG-835) were included. Afatinib was obtained from the DGIdb gene drug interaction database, while the latter two came from the Gene Cards database as EGFR inhibitors. These control drugs were chosen based on their superior characteristics among each generation of approved EGFR inhibitors [17]. Three-dimensional structures of both control drugs and the additional compounds were downloaded from PubChem (https://pubchem.ncbi.nlm.nih.gov/) and optimized for docking using Avogadro [48] with the Generalized Amber Force Field (GAFF) with 5000 steps.

To validate the docking procedure and classify the results, the docking was repeated ten times for each of the final 23 compounds, this time with an exhaustiveness of 30 to compensate for the large search space. The average binding energy was calculated for each compound. Using these results, along with the data from the OSIRIS software, a simple average score was obtained using the formula: Score = 1/4(solubility + drug-likeness + Drug score + |binding energy|). Solubility was left without taking the absolute value because, although it is negative, less negativity indicates better solubility, unlike binding energy.

2.4 Machine learning bioavailability prediction

Two machine learning models were implemented in this study. The first model was a regression model used to predict the pIC50 values of the final compounds. The second model was a classification model used to predict the bioavailability class of the compounds, whether they are active or non-active, independent of the pIC50 values. The intention behind using these two models was to complement each other and provide more robust predictions.

To train these models, data was downloaded from the ChEMBL database [49]. A search was conducted for compounds targeting human EGFR, and a dataset with the identifier CHEMBL203 was selected. The data included IC50 values in nanomoles for these compounds. Initially, there were 16,715 compounds in this dataset, but after data cleaning to remove zero or missing IC50 values, as well as duplicate or missing canonical SMILES, 9,508 compounds remained.

The compounds were then classified based on their IC50 values. Compounds with an IC50 value ≤ 1000 nm were classified as active, those with an IC50 value ≥ 10000 nm were classified as inactive, and the remaining compounds were classified as intermediate. The IC50 values were normalized to a cut-off value of 10^9 nm and converted into pIC50 values. Lipinski descriptors were calculated for these compounds, and a Mann-Whitney statistical test was applied to verify if the active and inactive classes belonged to different distributions.

Morgan fingerprints with a radius of 2 and 1024-bit vectors were obtained for these compounds using Python's RDKit package. The Random Forest algorithm was used as a regressor and classifier to train the models. The training set consisted of 80% of the available data, with the remaining 20% assigned to the test set. Model parameters were optimized through random search and cross-validation.

For the regression model, the pIC50 value was the objective variable (y), and the Morgan fingerprints were the independent variables (X). For the classification model, the pIC50 values were converted into a binary code: 1 for pIC50 ≥ 6 (active) and 0 for the rest (non-active, including inactive and intermediate). This binary code became the dependent variable, while the independent variables remained the same.

Once the models were trained, they were validated on the testing set and then applied to a final set of 23 compounds, including controls, obtained after ADMET filtering. The Python code used in this study is available in the supplementary materials.

A flowchart depicting the steps followed in this study is shown in Figure 2.

3 Results

The study yielded several significant findings. Firstly, six compounds with suitable characteristics for potential EGFR inhibitors were identified and classified. These compounds, in descending order based on their overall score, are: ZINC3816310 (Dovitinib), ZINC53683345 (Vandetanib), ZINC147701032, ZINC1494443 (Falnidamol), ZINC103297550, and ZINC20148984 (PP-121). Tables 1 and 2 provide detailed information about these compounds, along with the control drugs Afatinib, Almonertinib, and Erlotinib used for comparison. Additionally, Curcumin, Dimethylcurcumin, and Tirfostin-AG-835 obtained from drug databases were included for comparison.

The study also involved differential gene expression analysis, IPP networks, and hub genes. Figures 3 to 6 present the results of these analyses for both studies used. Notably, the EGFR hub gene exhibited the highest degree of interaction in both cases. Molecular docking results for the two highest-scoring compounds and Almonertinib (the control with the highest score) are summarized in Table 3. The remaining docking results can be found in the supplementary materials. Figures 7 to 9 illustrate the complexes derived from these docking analyses.

Enrichment analysis was performed using hub genes from the GSE25724 study, which demonstrated a superior interaction network (as depicted in Figure 6). The results from Enrichr and GeneTrail are presented in Figure 10. Notably, GeneTrail analysis

yielded identical top ten enriched categories regardless of whether the hub genes were directly uploaded, or the GEO accession number was provided. This consistency indirectly verifies the validity of the obtained hub genes. An important finding from the enrichment analysis is the involvement of EGFR in pancreatic cancer signaling pathways. Among the set of hub genes, EGFR, ERBB2, RAC1, MAPK3, and SMAD3 were found to participate in these pathways. The analysis also revealed sets of miRNAs associated with diabetes mellitus and pancreatic neoplasms, which are available in the supplementary materials. Figure 11 depicts the miRNA interaction network.

The results of the Mann-Whitney test for active and inactive compounds obtained from ChEMBL, classified based on Lipinski descriptors (molecular weight, octanol-water partition coefficient, number of hydrogen bond donors, and number of hydrogen bond acceptors), are presented in Table 4. It can be concluded that the compounds belong to different distributions, but both classes occupy the same chemical space, as shown in Figure 12.

Lastly, machine learning models were employed. The regression model achieved an R2 score of 0.73 and a MSE of 0.61. The classification model achieved an accuracy rate of 85% for classifying non-active compounds (inactive and intermediate) and an accuracy rate of 89% for classifying active compounds. The average precision rate was 87%, and the AUC value was 0.86. Figure 13 displays the corresponding graphs.

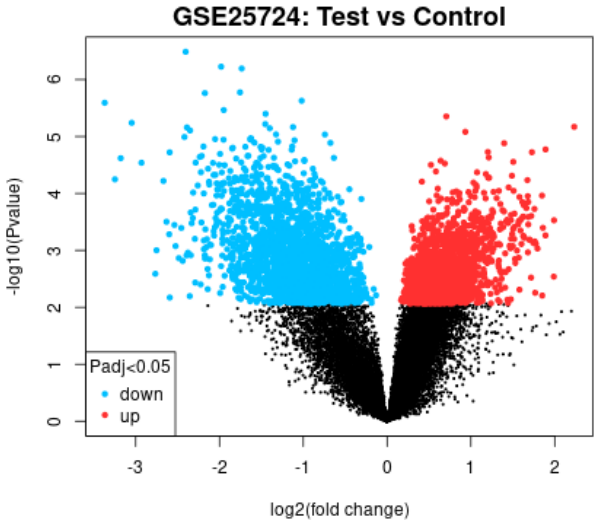

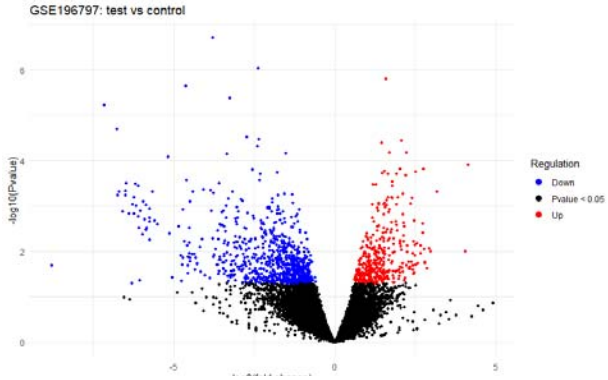

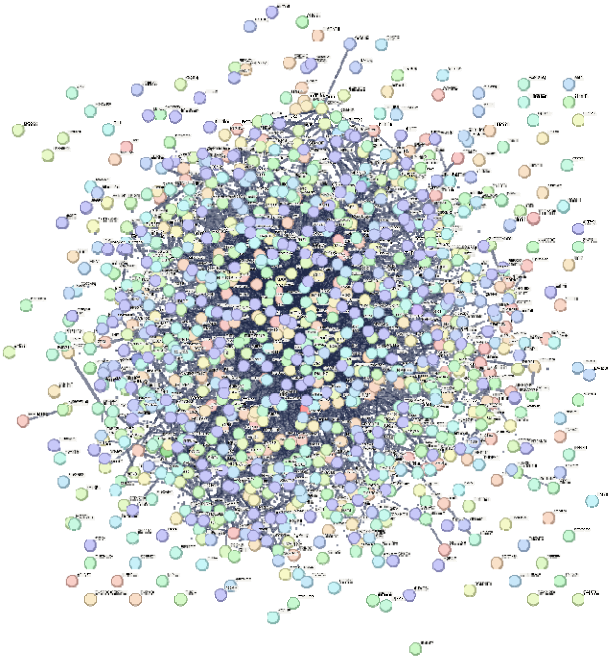

Figure 3. Volcano graphs for the differentially expressed genes in both studies.

Figure 4. Protein-Protein Interaction (PPI) network for the up-regulated genes in the GSE25724 study. It consists of 998 nodes and 5036 edges, with an average node degree of 10.1 and an average local clustering coefficient of 0.338. The expected number of edges is 4699, with a PPI enrichment p-value of 5.99e-07.

Figure 5. PPI network for up-regulated genes in study GSE196797. It consists of 298 nodes and 314 edges, with an average node degree of 2.11 and an average local clustering coefficient of 0.314. The expected number of edges is 229 with a PPI enrichment p-value of 6.37e-08.

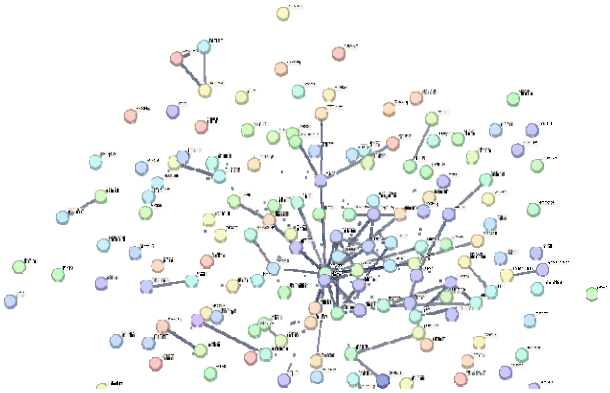

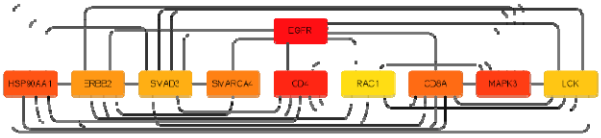

(a) Top ten hub genes from GSE25724

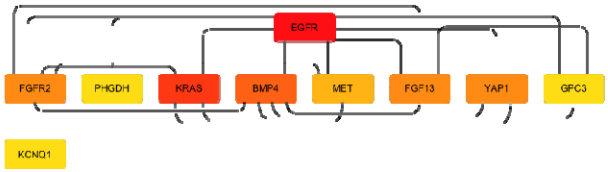

(b) Top ten hub genes from GSE196797

Figure 6. The top ten hub genes with the highest degree of interaction in the PPI network for both studies. Color code for the degree of interaction: darker red for the highest, lighter yellow for the lowest.

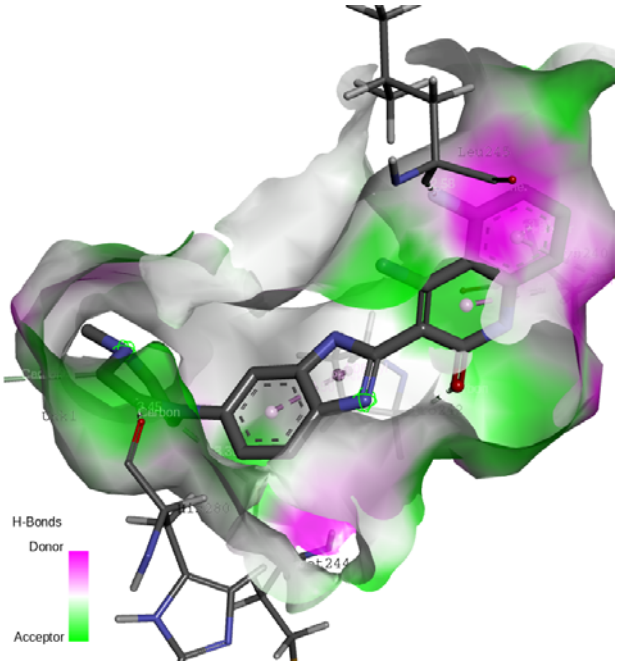

(a) Three-dimensional diagram based on the characteristics of donor-receptor hydrogen bonds between amino acid residues.

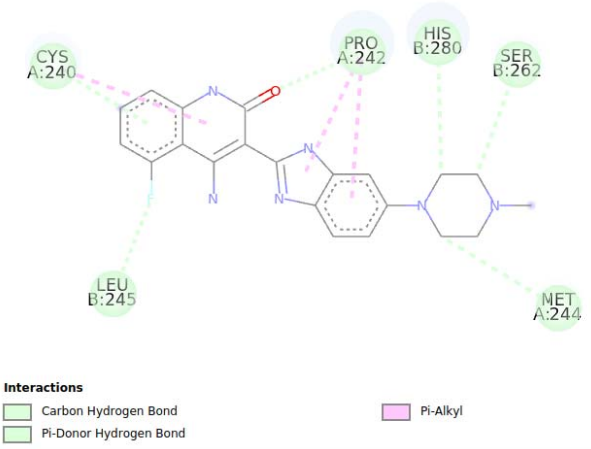

(b) Two-dimensional diagram showing various interactions between the ligand and the protein.

Figure 7. Molecular interactions for the complex EGFR-Dovitinib

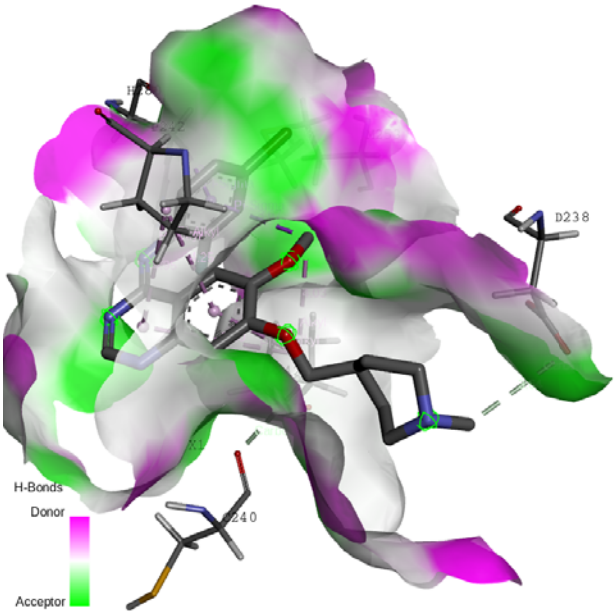

(a) Three-dimensional diagram based on the characteristics of donor-receptor hydrogen bonds between amino acid residues.

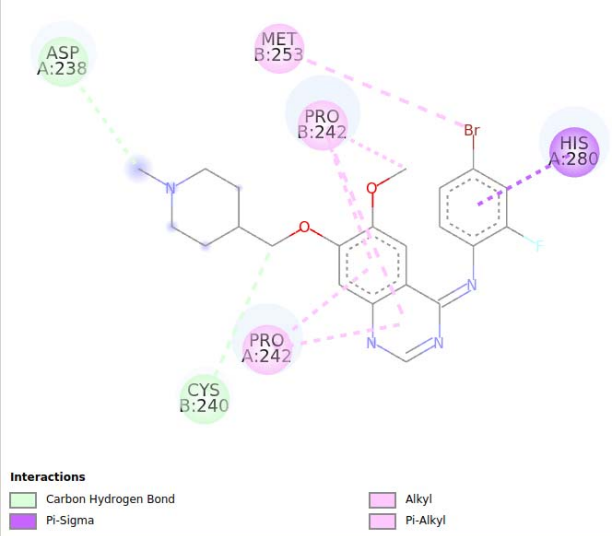

(b) Two-dimensional diagram showing various interactions between the ligand and the protein

Figure 8. Molecular interactions for the complex EGFR-Vandetanib

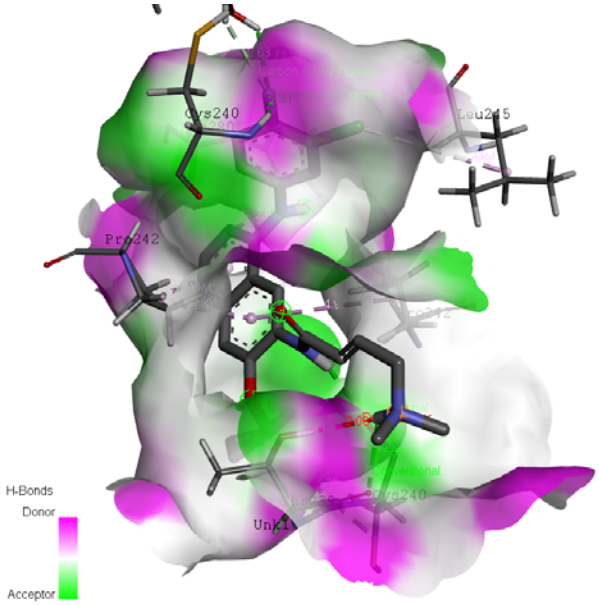

(a) Three-dimensional diagram based on the characteristics of donor-receptor hydrogen bonds between amino acid residues.

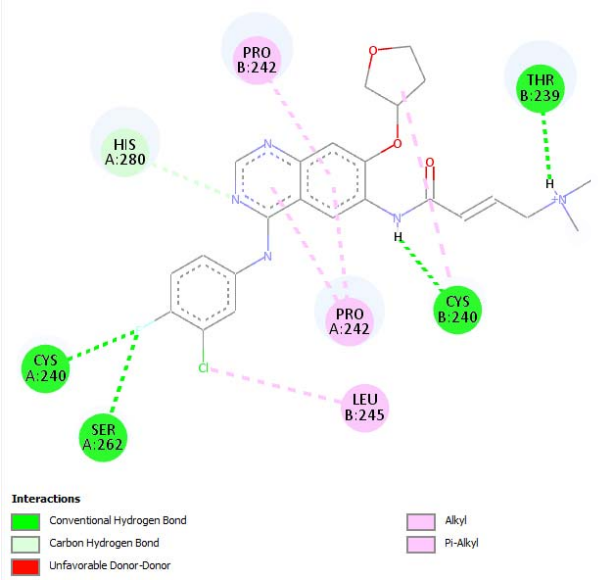

(b) Two-dimensional diagram showing various interactions between the ligand and the protein

Figure 9. Molecular interactions for the complex EGFR-Almonertinib

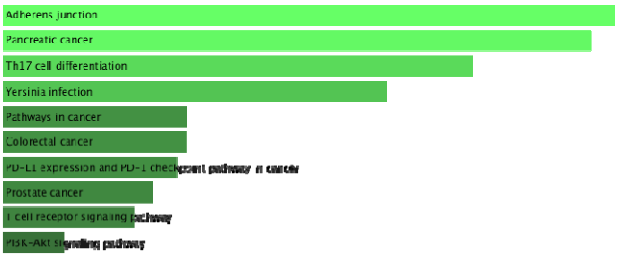

(a) Results from enrichment analysis against Kegg 2021 database. P-values are, respectively, 1.21e-10, 1.72e-10, 9.84e-10, 3.44e-09, 6.53e-08, 6.56e-08, 7.54e-08, 1.07e-07, 1.41e-07 and 3.96e-07.

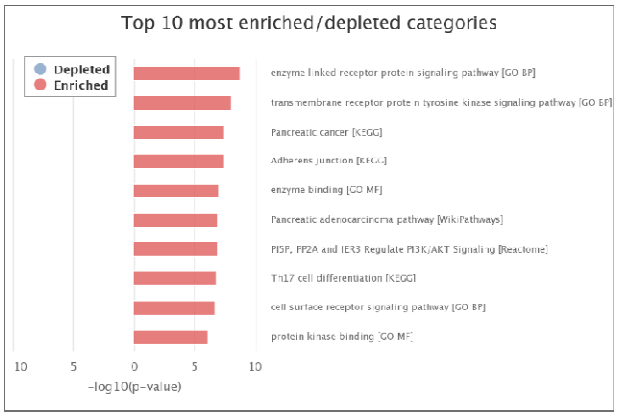

(b) Results from Gene Trail for the ten most enriched classes

Figure 10. Results from enrichment analysis of the ten hub genes from GSE25724

Table 1. Compounds properties. The Average column shows the average binding energy from the ten molecular docking runs, in kcal/mol. SD is the associated standard deviation. Solubility, Drug-likeness, and Drug Score are the scores obtained from OSIRIS Property Explorer. The final score is calculated using the formula 1/4(solubility + drug-likeness+ drug score + |binding energy|). The pIC50 column contains the numerical values predicted by the machine learning regression model, and Class represents the corresponding classification explained in section 2.5 (after conversion to IC50 values). The Classification column displays the results from the machine learning classifier model.

Compound	Canonical SMILES	Average binding energy	SD	Solubility	Drug likeness	Drug score	Final score	pIC50	Class	Classification
ZINC000003816310	CN1CCN(CC1)c1ccc2c(c1)[nH]c(n2)c1c(=O)[nH]c2c(c1N)c(F)ccc2	-9.69	0.25	-2.39	5.77	0.85	3.48	5.94	Intermediate	Non-active
ZINC000053683345	COc1cc2c(cc1OCC1CCN(CC1)C)[nH]cn /c/2=N /c1ccc(cc1F)Br	-8.86	0.02	-5.19	3.87	0.52	2.01	6.31	Active	Active
Dimethylcurcumin	COc1nccc(n1)c1c(ncn1[C@@H]1CC[C@@H](CC1)O)c1ccc(cc1)F	-8.02	0.24	-4.3	3.68	0.62	2.00	4.97	Inactive	Non-active
ZINC000147701032	COc1nccc(n1)c1c(ncn1[C@@H]1CC[C@@H](CC1)O)c1ccc(cc1)F	-9.19	0.53	-3.36	0.89	0.66	1.85	7.08	Active	Active
Tyrphostin-AG-835	N#C /C(=C \c1ccc(c(c1)O)O) /C(=O)N[C@H](c1cccc1)C	-8.68	0.01	-3.07	0.73	0.73	1.77	5.43	Intermediate	Non-active
ZINC000001494443	CN1CCC(CC1)Nc1ncc2c(n1)c(ncn2)Nc1ccc(c(c1)Cl)F	-8.75	0.40	-4.68	2.23	0.63	1.73	8.35	Active	Active
ZINC000103297550	Oc1cccc(c1)Nc1ccnc2c1c1cccc1[nH]2	-8.81	0.01	-4.97	0.56	0.54	1.23	6.27	Active	Active
Curcumin	COc1cc(C=CC(=O)CC(=O)C=C2ccc(c(c2)OC)O)ccc1O	-9.12	0.08	-3.62	-3.95	0.4	0.49	5.02	Intermediate	Non-active
ZINC000020148984	COc1cccc(c1)c1cn(c2c1c(N)ncn2)c1ccccc1	-8.98	0.02	-7.98	-0.35	0.33	0.24	6.20	Active	Active
Almonertinib	C=CC(=O)Nc1cc(Nc2nccc(n2)c2cn(c3c2cccc3)C2CC2)c(cc1N(CCN(C)C)C)OC	-8.60	0.33	-4.46	-4.09	0.08	0.03	9.17	Active	Active
Afatinib	CN(CC=CC(=O)Nc1cc2c(ncnc2cc1OC1COCC1)Nc1ccc(c(c1)Cl)F)C	-9.19	0.83	-5.48	-4.11	0.24	-0.04	8.62	Active	Active
Erlotinib	COCCOc1cc2c(ncnc2cc1OCCOC)Nc1cccc(c1)C#C	-7.84	0.32	-3.53	-6.73	0.38	-0.51	6.42	Active	Non-active

Table 2: Drug likeness properties. Molecular weight (MW) in g/mol, topological surface area (TPSA) in Å^2, brain blood barrier permeability (BBB). The Lipinski, Ghose, Veber, Egan and Muegge columns indicate the number of violations of the respective rules. The columns PAINS (Pan Assays Interference Structures), Brenk and Lead likeness indicate the number of alerts of the corresponding conditions.

Compound	MW	TPSA	BBB	Lipinski	Ghose	Veber	Egan	Muegge	PAINS	Brenk	Lead likeness
ZINC000003816310	392.43	94.04	No	0	0	0	0	0	0	0	1
ZINC000053683345	475.35	62.74	Yes	0	0	0	0	0	0	0	2
Dimethylcurcumin	396.43	74.22	Yes	0	0	0	0	0	0	3	3
ZINC000147701032	368.40	73.06	Yes	0	0	0	0	0	0	0	1
Tyrphostin-AG-835	308.33	95.35	No	0	0	0	0	0	1	3	0
ZINC000001494443	387.84	78.86	Yes	0	0	0	0	0	0	0	1
ZINC000103297550	257.30	60.94	Yes	0	0	0	0	0	0	0	1
Curcumin	368.38	93.06	No	0	0	0	0	0	0	2	2
ZINC000020148984	316.36	65.96	Yes	0	0	0	0	0	0	0	1
Almonertinib	525.64	87.55	No	1	3	1	0	0	0	1	3
Afatinib	485.94	88.61	No	0	1	0	0	0	0	1	3
Erlotinib	393.44	74.73	Yes	0	0	0	0	0	0	1	2

Table 3: Binding energy and type of molecular interaction for the top two finalist compounds dovitinib and vandetanib and the control almonertinib. The distance is reported in Å^2, and UNL1 refers to the corresponding ligand in each case.

Compound	Binding energy (Kcal/mol)	Donnor	Distance	Acceptor	Category	Interaction type
ZINC000003816310	-9.73	UNL1:C	2.99	B:SER262:OG	Hydrogen Bond	Carbon Hydrogen Bond
		UNL1:C	3.45	B:HIS280:O	Hydrogen Bond	Carbon Hydrogen Bond
		UNL1:C	3.39	A:MET244:O	Hydrogen Bond	Carbon Hydrogen Bond
		UNL1	4.50	A:PRO242	Hydrophobic	Pi-Alkyl
		UNL1	4.08	A:PRO242	Hydrophobic	Pi-Alkyl
		A:PRO242:HA	2.36	UNL1:O	Hydrogen Bond	Carbon Hydrogen Bond
		UNL1	5.20	A:CYS240	Hydrophobic	Pi-Alkyl
		UNL1	4.92	A:CYS240	Hydrophobic	Pi-Alkyl
		B:LEU245:HA	2.58	UNL1:F	Hydrogen Bond; Halogen	Carbon Hydrogen Bond; Halogen (Fluorine)
ZINC000053683345	-8.86	UNL1	4.95	A:PRO242	Hydrophobic	Pi-Alkyl
		UNL1	4.25	A:PRO242	Hydrophobic	Pi-Alkyl
		UNL1	4.01	B:PRO242	Hydrophobic	Pi-Alkyl
		UNL1	5.30	B:PRO242	Hydrophobic	Pi-Alkyl
		UNL1:C	3.69	UNL1	Hydrophobic	Pi-Sigma
		A:HIS280:HB2	2.75	UNL1	Hydrophobic	Pi-Sigma
		UNL1:BR	5.38	B:MET253	Hydrophobic	Alkyl
		UNL1:C	4.03	B:PRO242	Hydrophobic	Alkyl
		UNL1:C	3.64	B:CYS240:O	Hydrogen Bond	Carbon Hydrogen Bond
		UNL1:C	3.64	A:ASP238:OD2	Hydrogen Bond	Carbon Hydrogen Bond
Almonertinib	-8.65	UNL1:HN	2.56	B:THR239:O	Hydrogen Bond	Conventional Hydrogen Bond
		UNL1:H	2.46	B:CYS240:O	Hydrogen Bond	Conventional Hydrogen Bond
		B:CYS240	5.25	UNL1	Hydrophobic	Alkyl
		B:THR239:HG1	2.08	UNL1:HN	Unfavorable r	Unfavorable Donor-Donor
		UNL1	4.91	B:PRO242	Hydrophobic	Pi-Alkyl
		UNL1	4.21	A:PRO242	Hydrophobic	Pi-Alkyl
		UNL1	4.97	A:PRO242	Hydrophobic	Pi-Alkyl
		UNL1:CL	5.03	B:LEU245	Hydrophobic	Alkyl
		A:CYS240:HN	2.44	UNL1:F	Hydrogen Bond;Halogen	Conventional Hydrogen Bond;Halogen (Fluorine)
		A:SER262:HB2	2.63	UNL1:F	Hydrogen Bond	Carbon Hydrogen Bond
		A:SER262:HG	2.71	UNL1:F	Hydrogen Bond;Halogen	Conventional Hydrogen Bond;Halogen (Fluorine)

Table 4. Mann-Whitney test results (α = 0.05) for active and inactive compounds, from ChEMBL, for their Lipinski descriptors: Molecular weight (MW), Octanol – water partition coefficient (LogP), number of Hydrogen bond donors and acceptors. In all cases the null hypothesis is rejected, and we conclude that the compounds belong to different distributions.

Descriptor	Statistic	P value	Result
MW	8924972.0	1.38e-192	reject H0
LogP	7761898.5	4.09e-64	reject H0
NumHDonors	6906548.0	1.48e-15	reject H0
NumHAcceptors	8671850.5	7.33e-162	reject H0

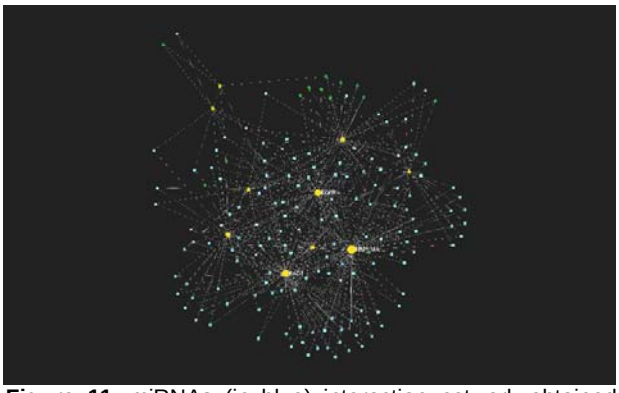

Figure 11. miRNAs (in blue) interaction network obtained from miRNet using the hub genes (in yellow) from the GSE25724 study.

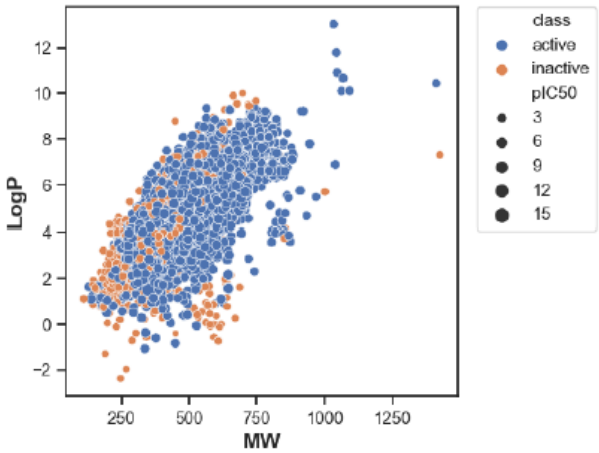

Figure 12. Scatter plot of molecular weight (MW) vs octanol water partition coefficient (LogP) for active and inactive compounds obtained from ChEMBL. The plot demonstrates that both classes occupy the same chemical space despite originating from different distributions based on their Lipinski descriptors.

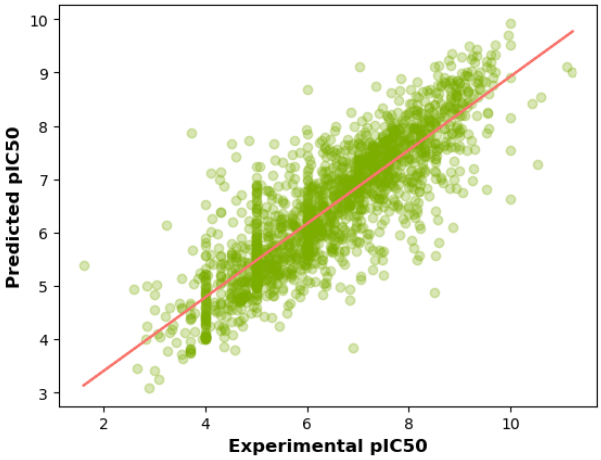

(a) Scatter plot of predicted vs actual results for pIC50 values obtained using the random forest regression model.

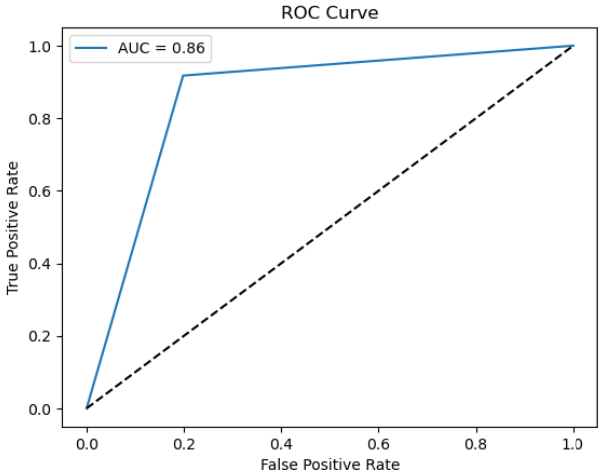

(b) ROC curve and area under the curve (AUC) for the random forest classification model.

Figure 13. Performance plots for both machine learning models.

3 Conclusions

An analysis of the data in Table 1 reveals that compound dovitinib obtained the highest score, with a pIC50 value of 5.94 according to the regression model. However, it was classified as non-active by the classification model. This suggests that dovitinib lies on the borderline between active and intermediate compounds. Given its favorable characteristics, it emerges as the top candidate for further development as a lead compound. Notably, dovitinib is currently being investigated for the treatment of multiple myeloma and solid tumors, as reported by Drug Bank.

The second-ranked compound, vandetanib, has already been approved for the treatment of symptomatic or progressive medullary thyroid cancer. This compound was classified as active by both models. These results open the possibility of repurposing these drugs for the treatment of type 2 diabetes and potentially pancreatic cancer.

To the best of our knowledge, the remaining four compounds are not currently under active investigation, except for falnidamol, which is known to be an orally active EGFR inhibitor. All these compounds were classified as active by both models, and their priority for development follows the order presented here based on their scores.

Regarding the ML models, the regression model slightly underperformed, as indicated by the difference between the Mean Squared Error (MSE) and R-squared values, which is approximately 10%. Various fingerprints, molecular descriptors, and feature selection techniques such as LASSO regression and PCA were explored for the independent variables. Based on the data available, the presented model was determined to be the best one. However, the classifier model performed better, and their combined use resulted in more robust predictions, as demonstrated by the presented results.

It is worth noting that all six finalist compounds achieved significantly better scores compared to the control drugs, which exhibited poor performance. Curcumin, despite having a good overall score, did not fall within the active range and cannot be considered a viable compound. The same holds true for tyrphostin-AG-835, and dimethylcurcumin displayed even worse bioactivity.

Another significant finding is the association of the EGFR gene with diabetes, independent of epigenetic studies. Although experimental validation is required, our results provide support to existing studies that have reported this association, as mentioned in the introduction. Moreover, the enrichment analysis revealed the involvement of EGFR in the signaling pathway of pancreatic cancer. In summary, these findings strengthen the association between EGFR and type 2 diabetes and confirm the achievement of our objective to identify potential drug candidates for its treatment. The narrowed-down viable hits from this study can now be further investigated in vitro. Additionally, since EGFR is a well-known oncogene, these results serve as a foundation for the development of improved drugs for diseases requiring its inhibition.

References

[1] DeFronzo RA, Ferrannini E, Groop L, Henry RR, Herman WH, Holst JJ, et al. Type 2 diabetes mellitus. Nature Reviews Disease Primers. 2015 Jul;1(1):15019.

[2] Galicia-Garcia U, Benito-Vicente A, Jebari S, Larrea-Sebal A, Siddiqi H, Uribe KB, et al. Pathophysiology of Type 2 Diabetes Mellitus. Int J Mol Sci. 2020 Aug;21(17).

[3] Goyal R, Jialal I. Type 2 diabetes - stat- pearls - NCBI bookshelf. Treasure Island (FL): StatPearls Publishing; 2023. Available from: https://www.ncbi.nlm.nih. gov/books/NBK513253.

[4] Hu F, Qiu X, Bu S. Pancreatic islet dysfunction in type 2 diabetes mellitus. Archives of Physiology and Biochemistry. 2020;126(3):235-41. PMID: 30293453. Available from: https://doi.org/10.1080/ 13813455.2018.1510967.

[5] Marchetti P, Del Guerra S, Marselli L, Lupi R, Masini M, Pollera M, et al. Pancreatic Islets from Type 2 Diabetic Patients Have Functional Defects and Increased Apoptosis That Are Ameliorated by Metformin. The Journal of Clinical Endocrinology and Metabolism. 2004 11;89(11):5535-41.

[6] Da Silva Xavier G. The Cells of the Islets of Langerhans. Journal of Clinical Medicine. 2018;7(3). Available from: https://www. mdpi.com/2077-0383/7/3/54.

[7] Böni-Schnetzler M, Meier DT. Islet in- flammation in type 2 diabetes. Seminars in Immunopathology. 2019 Jul;41(4):501-13. Available from: https://doi.org/10.1007/ s00281-019-00745-4.

[8] Goodarzi MO, Palmer ND, Cui J, Guo X, Chen YDI, Taylor KD, et al. Classification of Type 2 Diabetes Genetic Variants and a Novel Genetic Risk Score Association With Insulin Clearance. The Journal of Clinical Endocrinology 'I&' Metabolism. 2019 11;105(4):1251-60. Available from: https://doi.org/10.1210/clinem/dgz198.

[9] Shoily SS, Ahsan T, Fatema K, Sajib AA. Common genetic variants and pathways in diabetes and associated complications and vulnerability of populations with different ethnic origins. Scientific Reports. 2021 Apr;11(1):7504. Available from: https:// doi.org/10.1038/s41598-021-86801-2.

[10] ElHajj Chehadeh S, Sayed NS, Abdelsamad HS, Almahmeed W, Khandoker AH, Jelinek HF, et al. Genetic Variants and Their Associations to Type 2 Diabetes Mellitus Complications in the United Arab Emirates. Frontiers in Endocrinology. 2022;12. Avail- able from: https://www.frontiersin.org/ articles/10.3389/fendo.2021.751885.

[11] Davies MJ, Aroda VR, Collins BS, Gabbay RA, Green J, Maruthur NM, et al. Management of Hyperglycemia in Type 2 Diabetes, 2022. A Consensus Report by the American Diabetes Association (ADA) and the Euro- pean Association for the Study of Diabetes (EASD). Diabetes Care. 2022 09;45(11):2753-86. Available from: https://doi.org/10. 2337/dci22-0034.

[12] Artasensi A, Pedretti A, Vistoli G, Fuma- galli L. Type 2 Diabetes Mellitus: A Review of Multi-Target Drugs. Molecules. 2020;25(8). Available from: https://www. mdpi.com/1420-3049/25/8/1987.

[13] Reed J, Bain S, Kanamarlapudi V. A Re- view of Current Trends with Type 2 Dia- betes Epidemiology, Aetiology, Pathogenesis, Treatments and Future Perspectives. Dia- betes Metab Syndr Obes. 2021 Jun;14:3567- 602.

[14] Yarden Y, Pines G. The ERBB network: at last, cancer therapy meets systems biology. Nature Reviews Cancer. 2012 Aug;12(8):553-63. Available from: https://doi.org/10. 1038/nrc3309.

[15] Li Z, Li Y, Overstreet JM, Chung S, Niu A, Fan X, et al. Inhibition of Epidermal Growth Factor Receptor Activation Is Associated With Improved Diabetic Nephropathy and Insulin Resistance in Type 2 Diabetes. Diabetes. 2018

06;67(9):1847-57. Available from: https://doi.org/10.2337/db17-1513.

[16] Sheng L, Bayliss G, Zhuang S. Epidermal Growth Factor Receptor: A Potential Therapeutic Target for Diabetic Kidney Disease. Frontiers in Pharmacology. 2021;11. Available from:https://www.frontiersin.org/articles/10.3389/fphar.2020.598910.

[17] Abourehab MAS, Alqahtani AM, Youssif BGM, Gouda AM. Globally Approved EGFR Inhibitors: Insights into Their Syntheses, Target Kinases, Biological Activities, Recep- tor Interactions, and Metabolism. Molecules. 2021;26(21). Available from: https://www. mdpi.com/1420-3049/26/21/6677.

[18] Shannon P, Markiel A, Ozier O, Baliga NS, Wang JT, Ramage D, et al. Cytoscape: A Software Environment for Integrated Models of Biomolecular Interaction Net- works. Genome Research. 2003;13(11):2498-504. Available from: http://genome.cshlp. org/content/13/11/2498.full.html.

[19] Chin CH, Chen SH, Wu HH, Ho CW, Ko MT, Lin CY. cytoHubba: identifying hub objects and sub-networks from complex interactome. BMC Systems Biology. 2014 Dec;8(4):S11. Available from: https://doi.org/10.1186/ 1752-0509-8-S4-S11.

[20] Love MI, Huber W, Anders S. Moderated estimation of fold change and dispersion for RNA-seq data with DESeq2. Genome Biology. 2014 Dec;15(12):550. Avail- able from: https://doi.org/10.1186/ s13059-014-0550-8.

[21] Huber W, Carey VJ, Gentleman R, Anders S, Carlson M, Carvalho BS, et al. Orchestrating high-throughput genomic analysis with Bioconductor. Nature Methods. 2015 Feb;12(2):115-21. Available from: https://doi.org/10.1038/nmeth.3252.

[22] Chen EY, Tan CM, Kou Y, Duan Q, Wang Z, Meirelles GV, et al. Enrichr: interactive and collaborative HTML5 gene list enrichment analysis tool. BMC Bioinformatics. 2013 Apr;14:128.

[23] Kuleshov MV, Jones MR, Rouillard AD, Fernandez NF, Duan Q, Wang Z, et al. Enrichr: a comprehensive gene set enrichment analysis web server 2016 update. Nucleic Acids Res. 2016 May;44(W1):W90-7.

[24] Kanehisa M, Furumichi M, Sato Y, Ishiguro- Watanabe M, Tanabe M. KEGG: integrating viruses and cellular organisms. Nucleic Acids Research. 2020 10;49(D1):D545-51. Avail-able from: https://doi.org/10.1093/nar/ gkaa970.

[25] Backes C, Keller A, Kuentzer J, Kneissl B, Comtesse N, Elnakady YA, et al. GeneTrail – advanced gene set enrichment analysis. Nucleic acids research. 2007;35(suppl_2):W186- 92.

[26] Martens M, Ammar A, Riutta A, Waagmeester A, Slenter D, Hanspers K, et al. WikiPathways: connecting communities. Nucleic Acids Research. 2020 11;49(D1):D613-21. Available from: https://doi.org/10. 1093/nar/gkaa1024.

[27] Ashburner M, Ball CA, Blake JA, Botstein D, Butler H, Cherry JM, et al. Gene Ontology: tool for the unification of biology. Nature Genetics. 2000 May;25(1):25-9. Available from: https://doi.org/10.1038/75556.

[28] Consortium TGO, Aleksander SA, Balhoff J, Carbon S, Cherry JM, Drabkin HJ, et al. The Gene Ontology knowledgebase in 2023. Genetics. 2023 03;224(1):iyad031. Available from: https://doi.org/10.1093/ genetics/iyad031.

[29] Chang L, Xia J. In: Song Q, Tao Z, editors. MicroRNA Regulatory Network Analysis Us- ing miRNet 2.0. New York, NY: Springer US; 2023. p. 185-204. Available from: https:// doi.org/10.1007/978-1-0716-2815-7_14.

[30] Chang L, Zhou G, Soufan O, Xia J. miRNet 2.0: network-based visual analytics for miRNA functional analysis and systems biology. Nucleic Acids Research. 2020 06;48(W1):W244-51. Available from: https://doi.org/10.1093/nar/gkaa467.

[31] Consortium TU. UniProt: the Universal Pro- tein Knowledgebase in 2023. Nucleic Acids Research. 2022 11;51(D1):D523-31. Available from: https://doi.org/10.1093/nar/ gkac1052.

[32] Berman HM, Westbrook J, Feng Z, Gilliland G, Bhat TN, Weissig H, et al. The Protein Data Bank. Nucleic Acids Research. 2000 01;28(1):235-42. Available from: https://doi.org/10.1093/nar/28.1.235.

[33] Huang Y, Ognjenovic J, Karandur D, Miller K, Merk A, Subramaniam S, et al. A molecular mechanism for the generation of ligand- dependent differential outputs by the epidermal growth factor receptor. eLife. 2021 nov;10:e73218. Available from: https:// doi.org/10.7554/eLife.73218.

[34] Pettersen EF, Goddard TD, Huang CC, Couch GS, Greenblatt DM, Meng EC, et al. UCSF Chimera, A visualization system for exploratory research and analysis. Journal of Computational Chemistry. 2004;25(13):1605-12. Available from:https://onlinelibrary.wiley.com/doi/ abs/10.1002/jcc.20084.

[35] Guex N, Peitsch MC. SWISS-MODEL and the Swiss-Pdb Viewer: An environment for comparative protein modeling. ELECTROPHORESIS. 1997;18(15):2714-23. Available from:https://analyticalsciencejournals.onlinelibrary.wiley.com/doi/abs/10.1002/elps.1150181505.

[36] Irwin JJ, Tang KG, Young J, Dandarchuluun C, Wong BR, Khurelbaatar M, et al. ZINC20, A Free Ultralarge Scale Chemical Database for Ligand Discovery. Journal of Chemical Information and Modeling. 2020;60(12):6065-73. PMID: 33118813. Available from: https: //doi.org/10.1021/acs.jcim.0c00675.

[37] O'Boyle NM, Banck M, James CA, Morley C, Vandermeersch T, Hutchison GR. Open Babel: An open chemical toolbox. Journal of Cheminformatics. 2011 Oct;3(1):33. Available from: https://doi.org/10.1186/ 1758-2946-3-33.

[38] Trott O, Olson AJ. AutoDock Vina: Improving the speed and accuracy of docking with a new scoring function, efficient optimization, and multithreading. Journal of Computational Chemistry. 2010;31(2):455-61. Avail- able from: https://onlinelibrary.wiley. com/doi/abs/10.1002/jcc.21334.

[39] Eberhardt J, Santos-Martins D, Tillack AF, Forli S. AutoDock Vina 1.2.0: New Docking Methods, Expanded Force Field, and Python Bindings. Journal of Chemical Information and Modeling. 2021 Aug;61(8):3891-8. Avail- able from: https://doi.org/10.1021/acs. jcim.1c00203.

[40] Daina A, Michielin O, Zoete V. Swiss ADME: a free web tool to evaluate pharmacokinetics, drug-likeness and medicinal chemistry friend- liness of small molecules. Scientific Reports. 2017 Mar;7(1):42717. Available from: https://doi.org/10.1038/srep42717.

[41] Lipinski CA, Lombardo F, Dominy BW, Feeney PJ. Experimental and computational approaches to estimate solubility and permeability in drug discovery and development settings1PII of original article: S0169-409X(96)00423-1. The article was originally published in Advanced Drug Delivery Reviews 23 (1997) 3-25.1. Advanced Drug Delivery Reviews. 2001;46(1):3-26. Special issue dedicated to Dr. Eric Tomlinson, Advanced Drug Delivery Reviews, A Selection of the Most Highly Cited Articles, 1991-1998. Available from: https://www.sciencedirect.com/science/article/pii/S0169409X00001290.

[42] Ghose AK, Viswanadhan VN, Wendoloski JJ. A Knowledge-Based Approach in Designing Combinatorial or Medicinal Chemistry Libraries for Drug Discovery. 1. A Qual- itative and Quantitative Characterization of Known Drug Databases. Journal of Combinatorial Chemistry. 1999;1(1):55-68. PMID: 10746014. Available from: https://doi. org/10.1021/cc9800071.

[43] Veber DF, Johnson SR, Cheng HY, Smith BR, Ward KW, Kopple KD. Molecular Properties That Influence the Oral Bioavailability of Drug Candidates. Journal of Medicinal Chemistry. 2002;45(12):2615-23. PMID:12036371.Available from: https://doi. org/10.1021/jm020017n.

[44] Egan WJ, Merz KM, Baldwin JJ. Prediction of Drug Absorption Using Multivariate Statistics. Journal of Medicinal Chemistry. 2000;43(21):3867-77. PMID:

11052792. Available from: https://doi.org/10.1021/ jm000292e.
[45] Muegge I, Heald SL, Brittelli D. Simple Selection Criteria for Drug-like Chemical Matter. Journal of Medicinal Chemistry. 2001;44(12):1841-6. PMID: 11384230. Available from: https://doi.org/10.1021/ jm015507e.
[46] Delaney JS. ESOL: Estimating Aqueous Solubility Directly from Molecular Structure. Journal of Chemical Information and Computer Sciences. 2004 May;44(3):1000-5. Available from: https://doi.org/10.1021/ ci034243x.
[47] Ali J, Camilleri P, Brown MB, Hutt AJ, Kirton SB. Revisiting the General Solubility Equation: In Silico Prediction of Aqueous Solubility Incorporating the Effect of Topographical Polar Surface Area. Journal of Chemical Information and Modeling. 2012 Feb;52(2):420-8. Available from: https:// doi.org/10.1021/ci200387c.
[48] Hanwell MD, Curtis DE, Lonie DC, Vander- meersch T, Zurek E, Hutchison GR. Avogadro: an advanced semantic chemical editor, visualization, and analysis platform. Journal of Cheminformatics. 2012 Aug;4(1):17. Available from: https://doi.org/10.1186/ 1758-2946-4-17.
[49] Mendez D, Gaulton A, Bento AP, Chambers J, DeÂ Veij M, Félix E, et al. ChEMBL: towards direct deposition of bioassay data. Nucleic Acids Research. 2018 11;47(D1):D930-40. Available from: https://doi.org/10.1093/nar/gky1075.